Materials Chemistry and Physics 357 (2026) 132373

Contents lists available at ScienceDirect

Materials Chemistry and Physics

journal homepage: www.elsevier.com/locate/matchemphys

Systematic study of Zr^{4+}, Nb^{5+} and Mo^{6+} doping in $LiNi_{0.8}Mn_{0.1}Co_{0.1}O_2$ (NMC811) cathodes prepared from a commercial $Ni_{0.8}Mn_{0.1}Co_{0.1}(OH)_2$ precursor: Structural and electrochemical perspectives

Nur Anna Lia [a,b], Kelimah Elong [a,c], Farish Irfal Saaid [d], Lailatul Isti'adzah [a], Azira Azahidi [e], Nurul Dhabitah Basri [a], Nurul Atikah Mohd Mokhtar [f,g], Muhamad Kamil Yaakob [a,b], Muhd Firdaus Kasim [a,c,*]

[a] Centre for Functional Materials and Nanotechnology, Institute of Science, Universiti Teknologi MARA, 40450, Shah Alam, Malaysia
[b] School of Physics and Material Studies, Faculty of Applied Sciences, Universiti Teknologi MARA, 40450, Shah Alam, Malaysia
[c] School of Chemistry and Environment, Faculty of Applied Sciences, Universiti Teknologi MARA, 40450, Shah Alam, Malaysia
[d] Faculty of Applied Sciences, Universiti Teknologi MARA Pahang, Bandar Tun Abdul Razak Jengka, Pahang, 26400, Malaysia
[e] Faculty of Applied Sciences, Universiti Teknologi MARA Cawangan Sarawak, 94300, Kota Samarahan, Sarawak, Malaysia
[f] Department of Chemistry, Kulliyah of Science, International Islamic University Malaysia, Jalan Sultan Ahmad Shah, Bandar Indera Mahkota, 25200, Kuantan, Pahang, Malaysia
[g] Cell and Battery Test & Development, Global Development Campus, Dyson Manufacturing Sdn Bhd, 81400, Senai, Johor, Malaysia

HIGHLIGHTS

- Zr, Nb, Mo doped into $Ni_{0.8}Mn_{0.1}Co_{0.1}(OH)_2$ via solvent solution method.
- Cation mixing suppressed in all doped NMC811 samples.
- Zr^{4+}, Nb^{5+}, Mo^{6+} doping enhances electrochemical performance of NMC811.
- Zr-doped NMC delivers 199.27 mAh/g with 94.4% coulombic efficiency.
- Zr-doped NMC retains 71.6% capacity after 100 cycles at 0.1 C.

GRAPHICAL ABSTRACT

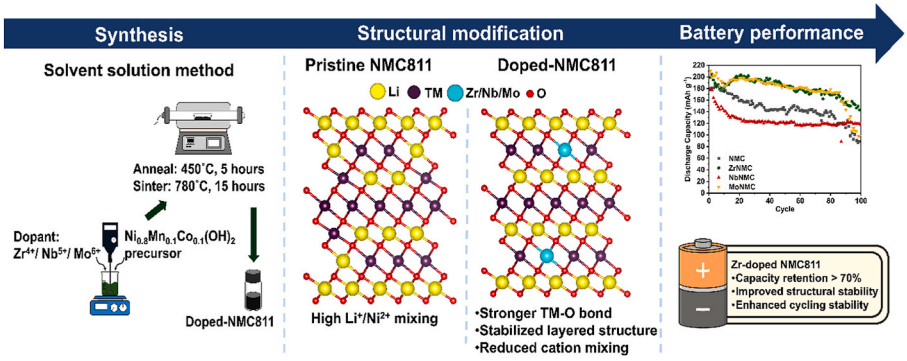

ARTICLE INFO

Keywords:
Lithium-ion batteries
Ni-rich cathodes
High oxidation state dopants
Zr doping
Nb doping
Mo doping

ABSTRACT

Lithium-ion batteries (LIBs) are widely used in energy storage due to their high energy density, long cycle life, and scalability. Nickel-rich lithium nickel manganese cobalt oxides (Ni-rich NMCs) are promising cathode materials owing to their high energy density. However, their application is limited by low stability, leading to capacity loss at high delithiated states and safety concerns. In this study, layered $LiNi_{0.8}Mn_{0.1}Co_{0.1}O_2$ (NMC811) cathode was doped with high oxidation state elements (Zr, Nb, and Mo), known for strong transition metal–oxygen (TM–O) bond energies. These dopants can hinder oxygen release and improve the chemical stability of Ni-rich cathodes. The materials were synthesized via a solvent solution method. X-ray diffraction (XRD)

* Corresponding author. Centre for Functional Materials and Nanotechnology, Institute of Science, Universiti Teknologi MARA, 40450, Shah Alam, Malaysia.
E-mail address: muhdfir@uitm.edu.my (M.F. Kasim).

https://doi.org/10.1016/j.matchemphys.2026.132373
Received 4 November 2025; Received in revised form 21 February 2026; Accepted 16 March 2026
Available online 17 March 2026

confirmed a single-phase layered structure without impurity peaks, and all doped samples showed an increased $I_{(003)}/I_{(104)}$ intensity ratio, indicating reduced cation mixing. No significant changes in particle morphology were observed due to the low dopant level (1 wt%). Electrochemical tests showed that Zr- and Mo-doped samples delivered higher initial discharge capacities and better cycling stability. Notably, Zr-doped NMC (ZrNMC) retained 71.6% of its capacity after 100 cycles at 0.1 C, compared to 49.6% for pristine NMC. Electrochemical impedance spectroscopy (EIS) revealed that ZrNMC exhibited lower charge transfer resistance during cycling, suggesting improved ion transport. These results indicate that doping with high oxidation state elements is an effective strategy to enhance the structural and electrochemical performance of Ni-rich NMC cathodes, making them more viable for next-generation LIB applications.

1. Introduction

In recent years, the global energy landscape has been shifting rapidly in order to address climate change, lower greenhouse gas emissions, and achieve carbon neutrality [1]. The extensive use of fossil fuels such as coal, oil, and natural gas has resulted in global warming, environmental harm, and growing concerns over energy security [2]. Nowadays, the shift towards renewable energy has been implemented to lessen dependence on non-renewable sources, such as solar, wind, biomass, geothermal, hydrogen energies and hydropower [3,4]. However, renewable energy generation is not always consistent and predictable due to their nature, causing low energy supply and cannot fulfill the energy demand [5,6]. Efficient and scalable energy storage systems are important for balancing the supply and demand, maintaining grid stability and facilitate integration of renewables into modern power systems [7,8].

Lithium-ion batteries (LIBs) have become a leading technology for energy storage applications due to high energy density, high lifespan, and scalability. Other than extensive use in portable electronics, electric vehicles (EVs), and hybrid electric vehicles (HEVs), LIBs are increasingly utilized in stationary energy storage systems that support renewable energy infrastructure [9]. The main component in LIBs is the cathode material, which significantly influences the battery's performance, including its discharge capacity, lifespan, and thermal stability [10,11]. Among the various cathode materials, nickel-rich lithium nickel manganese cobalt oxides (Ni-rich NMCs; Ni $\geq$ 60%) have gained a significant interest for their high energy density, cost efficiency and decreased reliance on cobalt as one of the main raw materials [12,13].

Despite their promising performance characteristics, Ni-rich NMC cathodes face several challenges that continue to impede the large-scale commercialization. One of the primary issues is their thermal instability, particularly at high states of charge, which raises safety concerns in commercial-scale applications such as EVs and grid storage [14]. In addition, increasing the nickel content often leads to structural degradation, including microcracking, phase transitions, and cation mixing between lithium and transition metal layers [14–16]. These phenomena result in capacity fading, cycling instability and shorten lifespan of the battery. To overcome these limitations, researchers have explored various strategies such as elemental doping, surface coatings, and synthesis process optimization to enhance the structural stability and electrochemical performance of Ni-rich NMC cathodes [17].

To overcome the structural and electrochemical limitations of Ni-rich NMC cathodes, one promising strategy involves the addition of foreign ion (dopant) elements into the layered structure of the cathode material. Recent studies have focused on optimizing dopant type to achieve a stability between high energy density and structural integrity. High oxidation states element such as Ti, Zr, Nb, V, and Mo has gained more attention due to their strong metal-oxygen bonds, which can suppress oxygen release and enhance the chemical stability of Ni-rich NMC cathodes [18–22]. Similar efforts in the literature have shown that high oxidation states element doped with Ni-rich cathode materials are more potent as a cathode stabilizer than low oxidation states dopant. Sun et al. found that doping $Li(Ni_{0.91}Co_{0.09})O_2$ cathode with Ta and Mo retain about 81.5% from their first cycle after 3000 cycles, and even alter the morphology of the cathode material. High oxidation states dopant acts as atomic pillars to prevent the collapse of layered planes when deeply charged [23].

To the best of our knowledge, no single experimental study has directly compared zirconium (Zr), niobium (Nb), and molybdenum (Mo) dopants in $LiNi_{0.8}Mn_{0.1}Co_{0.1}O_2$ (NMC811) using a commercial hydroxide precursor ($Ni_{0.8}Mn_{0.1}Co_{0.1}(OH)_2$), with all dopants introduced under identical synthesis conditions. Most prior studies rely on lab-synthesized precursors, which may complicate the interpretation results due to additional variables such as pH control, mixing, conditions, and chelating agents. Prior studies have typically focused on individual dopants. Extensive coprecipitation and coating investigations have been conducted for Zr [24–27]; Nb doping has also been examined in isolation [28–30]; and Mo doping has similarly been explored separately [31–33]. Most of these works apply different synthesis protocols for each dopant, making it difficult to systematically compare their effects on structural stability and electrochemical performance.

In addition, although solid state and co-precipitation methods are commonly used for doping method, few studies have investigated solvent based doping, particularly the solvent solution method using a commercial hydroxide precursor [19,22,23,34,35]. Colalongo et al. [36] compared two doping strategies, which are the dopant incorporation during co-precipitation synthesis, and addition of the dopant during the lithiation sintering step (solid-state synthesis). Their results showed that doping during the lithiation step led to the formation of significant phase-separated impurities, attributed to insufficient diffusion of Zr into NMC811 material. These findings highlight the importance of dopant incorporation at the precursor stage. Therefore, this work aims to incorporate Zr^{4+}, Nb^{5+}, and Mo^{6+} into $Ni_{0.8}Mn_{0.1}Co_{0.1}(OH)_2$ precursor via a solvent solution method followed by identical calcination steps, enabling a direct and quantitative comparison of their effects on crystal structure, particle morphology, and electrochemical performance. A commercial $Ni_{0.8}Mn_{0.1}Co_{0.1}(OH)_2$ precursor is deliberately employed as the baseline material to ensure reproducibility and industrial relevance, while eliminating uncertainties associated with precursor synthesis. This strategy allows multiple doped samples to be efficiently prepared from the same precursor. Thus, this study addresses a critical gap in the literature by establishing a unified doping strategy for preparing modified NMC811 using a commercially available precursor, offering a practical and scalable route for optimizing cathode materials without the need to synthesize the doped NMC hydroxide precursor from scratch.

2. Materials and methods

2.1. Synthesis of cathode materials

For the pristine sample, $LiNi_{0.8}Mn_{0.1}Co_{0.1}O_2$ was synthesized by using solid-state method. The precursor powder, $Ni_{0.8}Mn_{0.1}Co_{0.1}(OH)_2$ was obtained from commercial supplies (MSE Supplies). Firstly, the lithium hydroxide (LiOH) was added to $Ni_{0.8}Mn_{0.1}Co_{0.1}(OH)_2$ precursor powders in the container according to molar ratio of 1.10:1 which represent 10% mol of excess Li. The Li excess is to compensate Li loss during sintering and annealing process. LiOH and the precursor powder

were mixed homogenously by ball-milling process for 5 min over 4 cycles, using a 10 mm of zirconia (ZrO_2) balls. The obtained powder was then annealed at 450 °C for 5 h in a dry air atmosphere, followed by grinding and sintered at 780 °C for 15 h in an oxygen atmosphere. The final product was ground in the mortar to obtain a fine powder.

Doped $LiNi_{0.8}Mn_{0.1}Co_{0.1}O_2$ samples were synthesized by using a simple solvent solution method. In this process, 1 wt% of dopant was used to modify the NMC811 cathode material. Specifically, 1 wt% of zirconium oxynitrate hydrate ($ZrO(NO_3)_2{\cdot}xH_2O$), was first dissolved in distilled water, followed by the addition of ethanol at a distilled water-to-ethanol volume ratio of 1:5. The $Ni_{0.8}Mn_{0.1}Co_{0.1}(OH)_2$ precursor was then mixed with the dopant solution, homogenized with the speed of 600 rpm, and heated at 50–55 °C until complete evaporation. The resulting dry powder was left overnight in a drying oven. After drying, the doped precursor powder was mixed with LiOH, including a 10% molar excess of lithium to account for lithium loss via ball-milling process for 5 min over 4 cycles, using a 10 mm of zirconia (ZrO_2) balls. The dried doped precursor was then subjected to the same annealing and sintering steps as the pristine sample to produce the final doped NMC material. This process was repeated by using different source of dopant, which are ammonium niobate (V) oxalate hydrate ($C_4H_4NNbO_9{\cdot}xH_2O$), and ammonium molybdate tetrahydrate ($(NH_4)_6Mo_7O_{24}{\cdot}4H_2O$). The final products were designated as NMC, ZrNMC, NbNMC, and MoNMC. Fig. 1 illustrates the solvent solution method used for doping the NMC811 cathode.

2.2. Characterization

X-ray diffraction (XRD) was measured for both phase analysis and quantitative analysis. XRD data was conducted by using PANalytical X'pert Pro Diffraction instrument with Cu Kα X-ray radiation, operating at 40 kV and 30 mA. Diffraction data were collected over 15° to 90° for qualitative study and 15° to 150° for Rietveld refinement. The Rietveld refinement was performed by using X'pert HighScore Plus software. The morphology was examined by Field Emission Scanning Electron Microscopy (FESEM JEOL JSM-7600F instrument) with acceleration voltage of 5 kV. Elemental composition and distribution of the materials were determined by Energy-dispersive X-ray (EDX) (Oxford INCA X-Max 51-XMX 0021). Quantitative chemical compositions were determined through Inductively Coupled Plasma Mass Spectrometry (ICP-MS), using a PerkinElmer Elan 9000. Particle size distributions were measured with Laser Particle Sizer (FRITSCH Analysette 22 Nanotech).

2.3. Electrochemical measurements

Cathode electrodes were prepared from a slurry containing 88 wt % NMC811 active material, 6 wt % Super P conductive carbon, and 6 wt % poly(vinylidene fluoride) (PVDF) binder. The binder was dissolved first in N-Methyl-2-pyrrolidone (NMP) for 3 h at 50 °C. After 3 h, Super-P was then dispersed into the binder solution, followed by the gradual addition of NMC811 to obtain a homogeneous slurry. The uniform slurry was coated on aluminum foils, then dried at 80 °C in vacuum oven overnight. The dried coating was calendared and punched into circular electrodes. CR2032 coin-type cells were assembled in an Ar-filled glovebox using NMC811 as cathode, Li metal as an anode, and 1 M $LiPF_6$ electrolyte. Galvanostatic charge-discharge cycling was performed for 100 cycles, with a cycling voltage between 2.5 and 4.2 V (1 C = 180 mAh g^{-1}) with Wonatech WBCS-3000 tester. Electrochemical Impedance Spectroscopy (EIS) was carried out on a Wonatech WEIS510 Multichannel using 10 mV amplitude voltage and the frequency range of 0.01 - 1000 KHz. The EIS data was analyzed and fitted using Aftermath software by Pine Research Instrumentation.

3. Results and discussion

3.1. Phase and structural studies

Fig. 2a showed the structural studies for all materials and it was revealed that the diffraction peaks can be assigned to a hexagonal α-$NaFeO_2$ crystal structure with the R-3m space group (ICDD reference number: Lithium Nickel Oxide, 01-085-1967) indicating that the samples were pure and a single phase where no impurities were detected in any of the prepared materials, which demonstrate that Zr^{4+}, Nb^{5+} and Mo^{6+} ions have been successfully incorporated into the lattice layered of

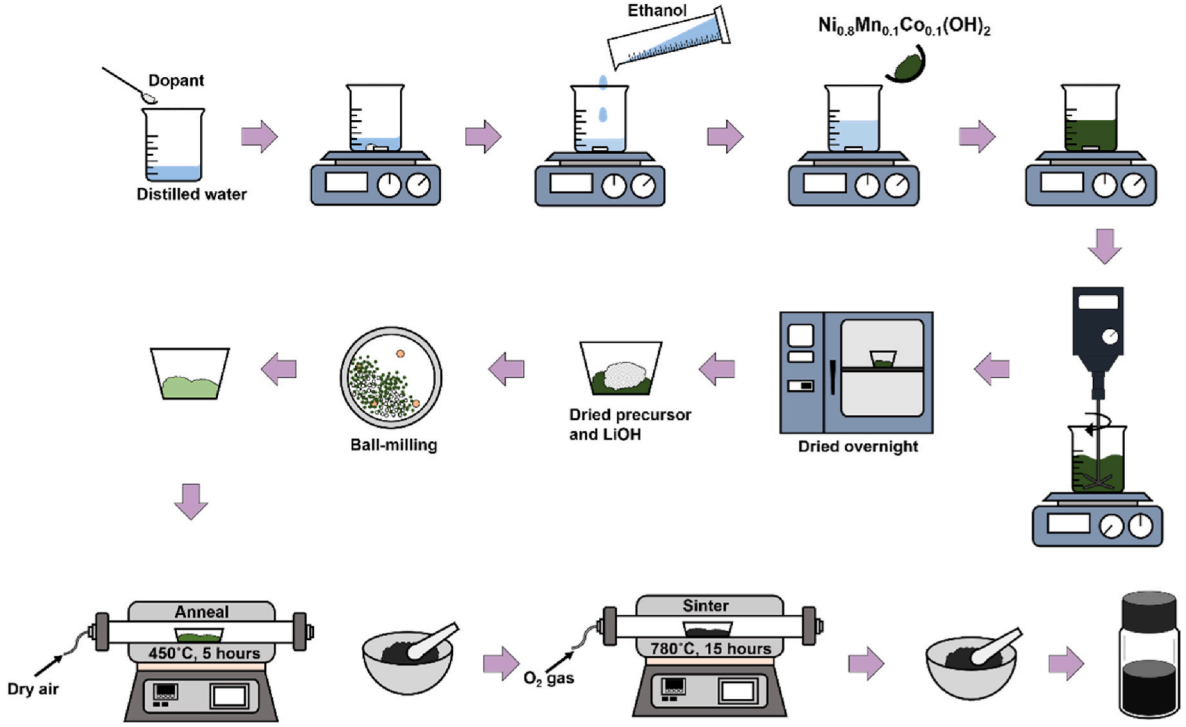

Fig. 1. Flowchart of the synthesis method for doped NMC811 samples.

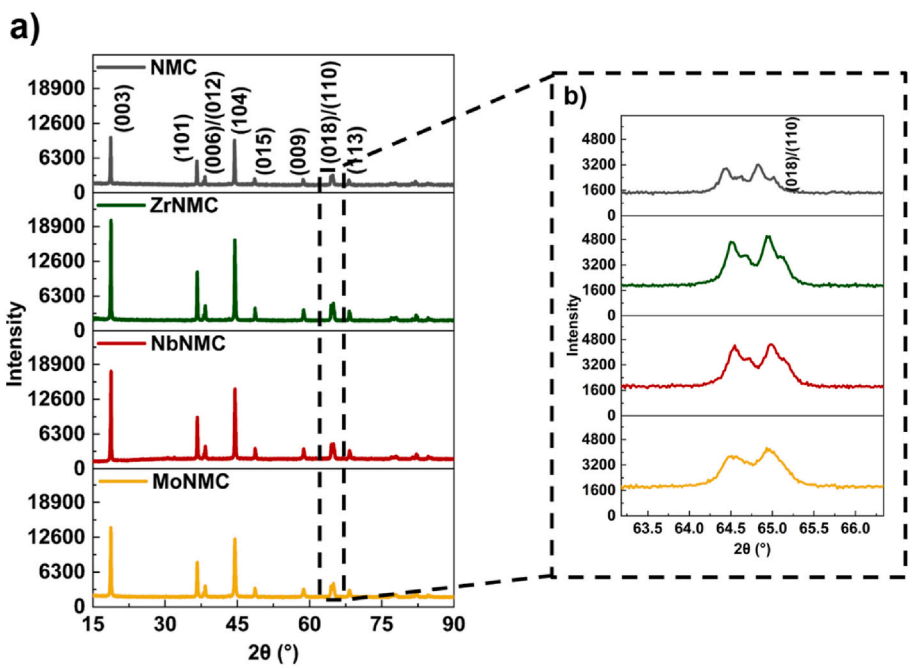

Fig. 2. (a) XRD profiles and (b) zoom-in view of (018/110) splitting peaks of NMC, ZrNMC, NbNMC and MoNMC.

NMC811 [37,38]. Upon closer inspection of the XRD patterns, it was observed that the intensity of cathode materials increased upon the incorporation of the dopant indicating an improvement in crystallinity [39]. The degree of cation mixing in the structure was evaluated using the XRD peak intensity ratio of the (003) to (104) reflections, known as the reference intensity ratio (RIR). It is well accepted that an RIR value greater than 1.2 indicates minimal cation mixing, which is associated with improved electrochemical performance [22,34]. The RIR values for pristine NMC, ZrNMC, NbNMC, and MoNMC were found to be 1.05, 1.26, 1.26, and 1.20, respectively. These results suggest that doping effectively reduces cation mixing and is likely to enhance electrochemical performance. Additionally, all synthesized samples exhibited clear splitting of the (006)/(102) and (018)/(110) peaks as shown in Fig. 2b, indicating a highly ordered layered structure which is critical for facilitating efficient lithium-ion diffusion and thus contributes to improved electrochemical performance [40,41].

The structural of the materials were further analyzed by Rietveld refinement shown in Fig. 3. The lattice parameters were tabulated in Table 1. The values of R_{wp} of all cathode materials are below 10%, indicating the result of the refinement is credible and reliable [40,42]. From Tables 1 and it can be observed that the lattice parameters along the a- and c-axis decrease upon the introduction of dopants into the NMC lattice. Although the ionic radii of Mo^{6+} (0.059 nm), Nb^{5+} (0.064 nm), and Zr^{4+} (0.076 nm) differ, the consistent reduction in lattice parameters suggests that the lattice evolution is not governed solely by dopant size. The incorporation of high-valence dopants likely induces charge redistribution within the transition metal (TM) layer, promoting partial oxidation of Ni^{2+} (0.069 nm) to Ni^{3+} (0.059 nm) to maintain charge neutrality [43] Since higher oxidation states correspond to smaller effective ionic radii, this charge compensation mechanism can result in lattice contraction. This interpretation is supported by the Rietveld refinement results, which reveal reduced Ni occupancy at the 3a site and increased c/a ratios in the doped samples compared to the pristine material. The decrease in Ni^{2+} concentration suppresses Li^{+}/Ni^{2+} cation mixing, thereby stabilizing the layered structure and contributing to the observed reduction in lattice volume. Furthermore, enhanced TM–O bond strength may contribute to lattice contraction. This occurs because the bond strengths of Zr–O (760 kJ/mol), Nb–O (753 kJ/mol), and Mo–O (560 kJ/mol) are significantly higher than those of Co–O (368 kJ/mol), Ni–O (391.6 kJ/mol), and Mn–O (402 kJ/mol) [22,30,44]. The stronger bonding between the dopant atoms and oxygen leads to a contraction of the lattice parameter resulting in a more compact and stable layered structure compared to pristine NMC. Therefore, the observed structural shrinkage reflects electronic and bonding effects rather than simple ionic radius considerations.

Interestingly, all doped samples exhibit a higher c/a ratio (>4.9) compared to the pristine sample, indicating better structural ordering and well-developed hexagonal structures, which can facilitate Li^{+} movement during cycling [45]. In the layered structure of NMC, Li occupies the 3a site, transition metals (Ni, Mn, and Co) occupy the 3b site, and oxygen occupies the 6*c* site [46]. To evaluate the degree of cation mixing between Ni^{2+} and Li^{+} ions, the site occupancy factor (s.o.f.) of Ni at the 3a site was analyzed, and the results are presented in Table 1. The percentage of cation mixing for NMC, ZrNMC, NbNMC, and MoNMC are 4.23%, 2.92%, 2.83%, and 3.52%, respectively. The analysis reveals that all doped samples exhibit lower cation mixing compared to the pristine NMC, which proves that strong TM-O bonds can suppress the cation mixing resulting in a more well-ordered layered structure. This improved ordering facilitates easier Li^{+} ion migration during the charge–discharge process, thereby enhancing the electrochemical performance of the cathode materials. Meanwhile, the slight increase of s.o.f. Ni at 3a sites for MoNMC is believed due to reduction of Ni^{3+} to Ni^{2+} to maintain charge neutrality within the structure. This result is correlated with the slight expansion of lattice parameter, indicate to the increase of Ni^{2+} that can migrate to the 3a site [47–49].

3.2. Morphology and elemental composition analysis

Fig. 4 shows the morphology, EDX and mapping result for all samples. The average secondary particles size for all samples was measured by particle sizer and the detailed distribution is listed in Table 2. All cathode materials possess a similar morphology of spherical secondary particles, which can be stated that the addition of foreign element (dopant) does not influence the morphology of the particles. Secondary particles were made of sub-μm sized primary particles attach together. It was found that, for dopant samples, the particle size distribution curve

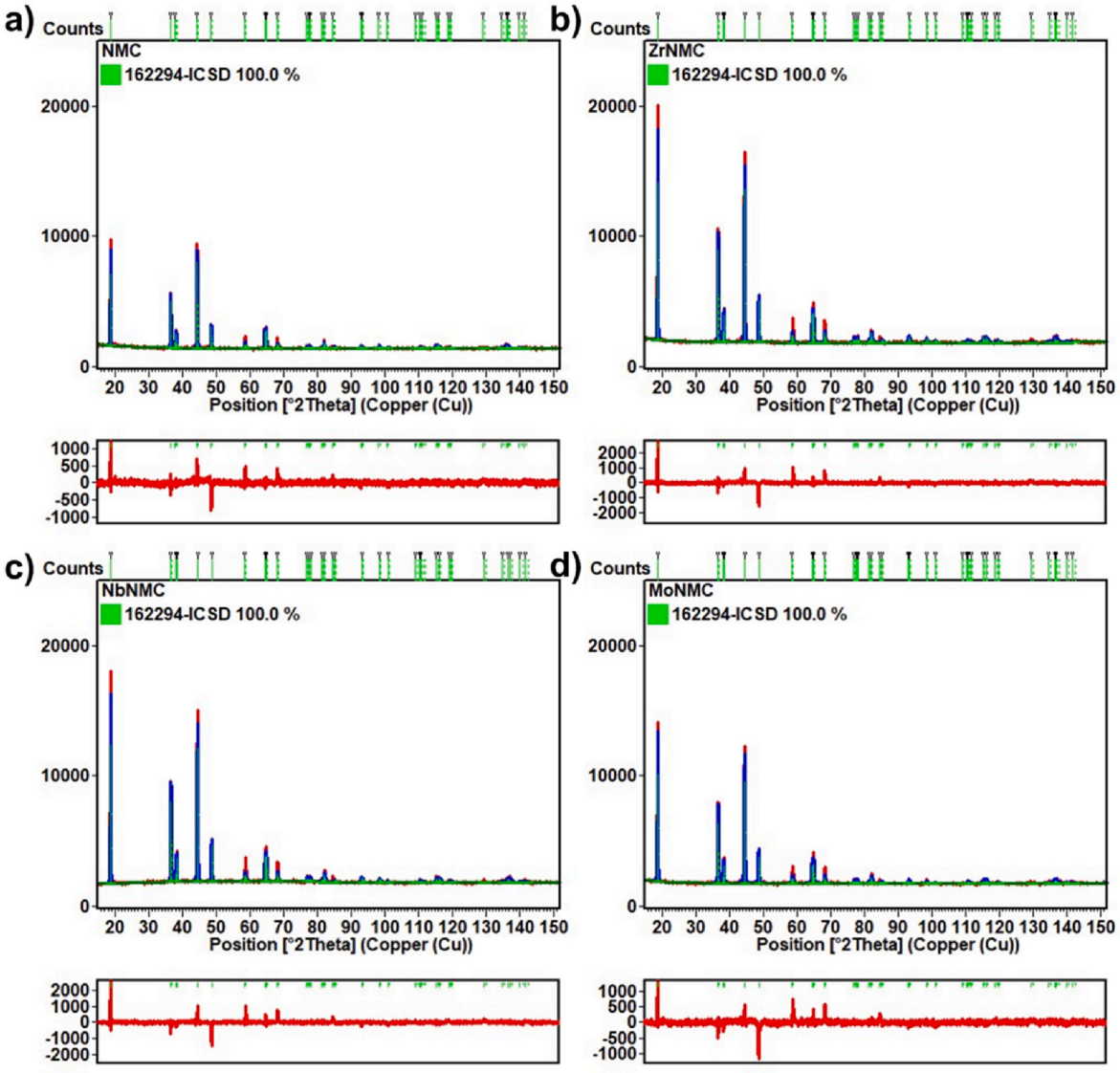

Fig. 3. Rietveld refinement of (a) NMC, (b) ZrNMC,(c) NbNMC, and (d) MoNMC.

Table 1
Crystallographic parameters of the NMC, ZrNMC, NbNMC and MoNMC materials calculated by the Rietveld refinements of the XRD data sets (s.o.f. = site of occupancy factor).

Sample	a = b (Å)	c (Å)	V (Å^3)	c/a	R_{wp}	s.o.f of Ni (3a)	s.o.f of Ni (3b)	s.o.f of Mn (3b)	s.o.f of Co (3b)	s.o.f of dopant (3b)	s.o.f of O (6c)	RIR
NMC	2.8713	14.1797	101.2387	4.9384	3.5746	0.04233	0.75767	0.10060	0.10063	-	1.0000	1.05
ZrNMC	2.8677	14.1738	100.9463	4.9426	4.2775	0.02917	0.77083	0.10070	0.10068	0.01046	1.0000	1.26
NbNMC	2.8668	14.1710	100.8610	4.9431	4.1253	0.02833	0.77167	0.10044	0.10450	0.01026	1.0000	1.26
MoNMC	2.8676	14.1786	100.9710	4.9444	3.8469	0.03519	0.76481	0.10101	0.10102	0.01025	1.0000	1.20

skews toward to the left indicating the particles size of the doped samples become smaller than pristine NMC. All secondary particles within the powders exhibited the spherical configurations, with an average size (D50) ranging from 11 to 14 μm. Generally, based on Table 2, the average of the particle size decreased when the dopant is added to the pristine sample. Commonly, cathode with smaller particle-size indicate shorter Li^+ diffusion length, thus, faster Li^+ diffusion [50]. To conclude, the particle size of all doped sample decreased, which will be expected the improvement of electrochemical performance. Mapping result shows that all samples have a uniform element distribution of Ni, Mn, Co and doped element.

To further confirm the elemental composition of doped samples, ICP-MS analysis was performed, and the results are tabulated in Table 3. The Li molar fraction was found to be greater than 1, which is attributed to the intentional addition of 10 mol.% excess Li to compensate for lithium loss during high-temperature synthesis. The dopant molar fractions listed in Table 3 confirm the successful incorporation of approximately 1 wt% of each dopant. Additionally, the measured Ni molar fraction is slightly higher than the nominal 80%. This observation is consistent with the precursor composition, as the commercial $Ni_{0.8}Mn_{0.1}Co_{0.1}(OH)_2$ precursor was found to have a Ni content slightly above 80%, despite the label specification.

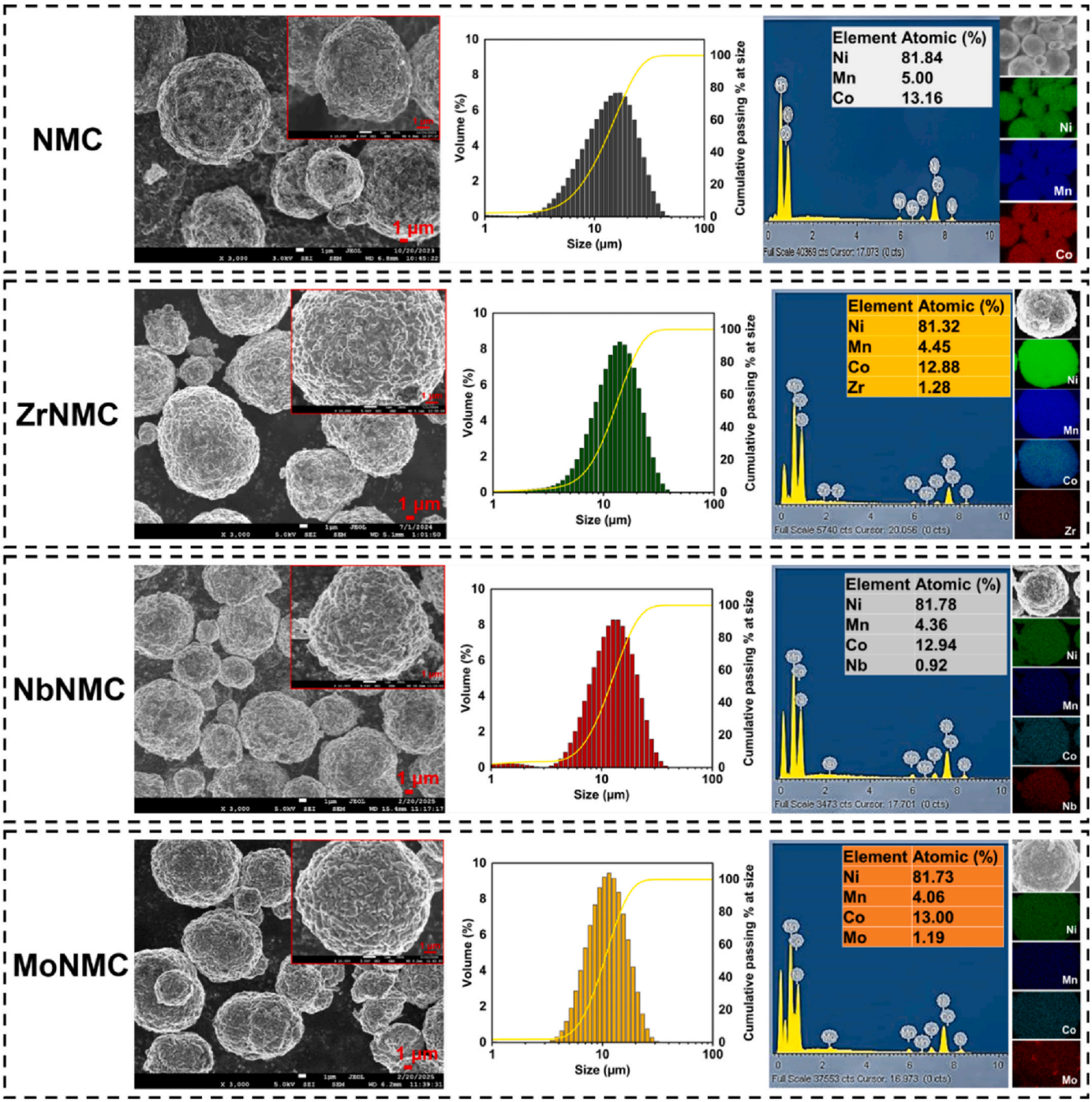

Fig. 4. SEM images, EDX and mapping of NMC, ZrNNC, NbNMC and MoNMC.

Table 2
Range and average size of secondary particles of NMC, ZrNMC, NbNMC and MoNMC.

Sample	NMC	ZrNMC	NbNMC	MoNMC
D10 (µm)	5.48	6.20	6.01	5.88
D50 (µm)	13.09	12.47	11.90	10.38
D90 (µm)	24.53	21.49	20.67	17.06
Mean diameter (µm)	14.37	13.37	12.86	11.11

3.3. Electrochemical performance of cathode materials

Fig. 5a presents the initial charge/discharge curves of all samples at a 0.1 C rate and Fig. 5b shows the cyclability of all samples for 100 cycles. The corresponding results are summarized in Table 4. The initial discharge capacities of NMC, ZrNMC, NbNMC, and MoNMC are 179.50, 199.27, 177.75, and 210.24 mAh g^{-1}, respectively. These results indicate that the initial discharge capacity generally increases with doping, except in the case of NbNMC. The relatively low discharge capacity of NbNMC can be attributed to its lattice parameters (Table 1). Specifically, NbNMC exhibits the smallest unit cell volume among all samples, indicating a more compact crystal structure. This compactness significantly hinders Li^+ diffusion, as more energy is required to extract Li^+ ions, thereby reducing ion mobility and overall capacity. The initial Coulombic efficiency (ICE) of all cathode materials was calculated and tabulated on Table 4 to observe the reversibility of the Li^+ ions and SEI

Table 3
ICP-MS analysis of NMC811 precursor, NMC, ZrNMC, NbNMC, MoNMC.

Sample	Li (mol. Fraction)	Ni (mol. Fraction)	Mn (mol. Fraction)	Co (mol. Fraction)	Dopant (mol. Fraction)
NMC811 precursor	-	0.8544	0.0471	0.0985	-
NMC	1.4720	0.8486	0.0519	0.0996	-
ZrNMC	1.6712	0.8517	0.0499	0.0974	0.0011
NbNMC	1.6484	0.8519	0.0494	0.0981	0.0006
MoNMC	1.7161	0.8494	0.0492	0.0971	0.0044

formation during charge and discharge at the first cycle [51]. It can be seen that ZrNMC shows the highest ICE, indicating to a larger portion of the battery's capacity is available for reversible charge/discharge cycles and moderate SEI formation inside the cell. Higher ICE contributes to better overall battery performance. Fig. 5b shows the cycling performance of all cathode materials over 100 cycles. It was found that ZrNMC exhibited an excellent cycling performance with the highest capacity retention, which is 71.6%. This result is consistent with its ICE. Meanwhile, although the discharge capacity of NbNMC remains relatively low throughout cycling, it does show slightly higher capacity than pristine NMC at the 100th cycle. The capacity remained stable starting from 20th to 100th cycle, indicating modest long-term improvement due to doping.

To understand the structural transformation and electrochemical reversibility of the cathode materials, differential capacity (dQ/dV) analysis was performed within a voltage range of 2.5–4.2 V, as shown in Fig. 5c–f. Each peak in the dQ/dV curves corresponds to a phase transition occurring at a specific voltage. It can be observed that the first oxidation peaks of the Zr- and Mo-doped samples shift to lower voltages compared to pristine NMC and NbNMC, indicating that less energy is required to initiate Li^+ ion migration. This facilitates the participation of more Li^+ ions during the initial cycles, resulting in a higher initial discharge capacity [30]. In contrast, the first oxidation peak of NbNMC (3.79 V) is nearly identical to that of pristine NMC (3.78 V), and their initial discharge capacities are also comparable. This behavior in NbNMC can be attributed to its more compact crystal structure, as previously discussed, which requires higher energy to initiate Li^+ ion diffusion, thereby limiting Li^+ participation during deintercalation.

In the second cycle, the oxidation peaks shift to lower potentials compared to the initial cycle, which is attributed to the irreversible capacity loss in the first cycle [52]. Moreover, the well-overlapped reduction peaks observed in all samples suggest that this irreversible loss is primarily due to the formation of a solid electrolyte interphase (SEI) layer. Ni-rich layered cathode materials, such as NMC, undergo a sequence of phase transitions during lithium extraction, starting from the original layered hexagonal structure (H1) to a monoclinic phase (M), followed by a second hexagonal phase (H2), and finally transitioning to a third hexagonal phase (H3) [22]. The H2/H3 transition, which occurs near 4.2 V, is widely regarded as the main contributor to capacity fading. This phase transition arises when most of the Li^+ ions have been extracted, leading to significant lattice shrinkage along the c-axis [35]. This shrinkage creates internal stress and weakens the structure, which speeds up the loss of battery capacity. As shown in Fig. 5c, the intensity of the H2/H3 transition peak for pristine NMC decreases progressively with cycling, indicating poor structural reversibility [53]. In contrast, the doped cathode materials retain more prominent H2/H3 transition peaks, especially in the case of ZrNMC (Fig. 5d). This suggests that the incorporation of dopants, particularly Zr^{4+}, enhances the structural stability and improves the electrochemical reversibility of the NMC cathode.

The potential differences (ΔE) between the cathodic and anodic peaks were calculated for the first cycle for all cathode materials to evaluate the degree of polarization [54]. The degree of polarization reflects the internal resistance of the cathode material; a lower polarization indicates low internal resistance and good charge transfer kinetics [55]. It was found that the ΔE values for NMC, ZrNMC, NbNMC, and MoNMC were 0.1041, 0.0038, 0.0772, and 0.0200 V, respectively.

Generally, polarization decreased after the addition of dopants. Among them, ZrNMC exhibited the lowest polarization, suggesting that the incorporation of Zr^{4+} ions improve the structural stability and reduces internal resistance of the cathode material. The low polarization of ZrNMC at the first cycle also shows that it has good reversibility in initial cycling [28].

The rate capability of each cathode materials was evaluated at varying current densities (0.1 C, 0.2 C, 0.5 C, 1.0 C and 2.0 C) within a voltage window of 2.5 V – 4.2 V as shown in Fig. 5g. The discharge capacity decreased with an increase of the current density, and the difference in discharge capacity performance among the cathode materials became more pronounced at high current densities. It was revealed that ZrNMC and MoNMC samples exhibited an excellent rate capability compared to NMC. At high density current of 2.0 C, the first discharge capacity of NMC, ZrNMC, NbNMC and MoNMC is 44.3 mAh g^{-1}, 115.4 mAh g^{-1}, 33.7 mAh g^{-1} and 117.9 mAh g^{-1}, respectively. ZrNMC and MoNMC show a major improvement in terms of high-rate current tests.

EIS tests were conducted on NMC, ZrNMC, NbNMC, and MoNMC before cycles and after 100th charge-discharge cycles and the Nyquist plots are shown in Fig. 6a and b respectively. In Fig. 6a, the Nyquist plots consist of a high-frequency intercept corresponding to the ionic resistance of the electrolyte (R_s) [56]. Before cycling, the Nyquist plot exhibits a single depressed semicircle followed by a low-frequency slanting line, indicating that the impedance response is mainly governed by the intrinsic charge-transfer resistance (R_{ct}) at the cathode/electrolyte interface. At this stage, no well-developed cathode–electrolyte interphase (CEI) has formed, and surface-related resistance is negligible [57]. The low frequency slanting line is related to the Li^+ ions diffusion in the electrode materials, namely Warburg impedance (Z_w). The fitted R_{ct} data are shown in Table 5. Before cycling, the R_{ct} value of ZrNMC (88.14 Ω) and MoNMC (42.49 Ω) are lower than that of pristine NMC (117.14 Ω), indicating reduced charge transfer resistance after element doping. This suggests more favorable initial electrochemical performance, consistent with the higher initial discharge capacity observed for the ZrNMC and MoNMC samples. In contrast, NbNMC exhibits a higher R_{ct} value than pristine NMC, indicating greater resistance to interfacial charge transfer. This increased interfacial resistance likely hinders the electrochemical reaction kinetics, providing an additional explanation for the lower initial discharge capacity of NbNMC.

Fig. 6b shows the Nyquist plots of all cathode materials after 100 charge-discharge cycles. After 100 cycles, two distinct semicircles emerge. The high-frequency semicircle is attributed to the resistance of the surface film (R_{sf}) formed during cycling, including CEI layers and surface reconstruction products typical of Ni-rich cathodes, while the medium-frequency semicircle corresponds to the R_{ct} [58]. The low-frequency sloping line in both cases is associated with Li^+ diffusion in the bulk cathode material. The pristine NMC exhibits pronounced impedance growth, particularly in the R_{sf} (131.7 Ω), along with a large R_{ct} (242.1 Ω). The high R_{sf} indicates severe surface degradation and substantial CEI formation, leading to the highest total interfacial resistance (R_{int} = 373.8 Ω). In contrast, ZrNMC shows a markedly lower R_{sf} (74.62 Ω) and R_{ct} (107.46 Ω), demonstrating that Zr doping effectively suppresses surface parasitic reactions and stabilizes the cathode–electrolyte interface during prolonged cycling, resulting in the

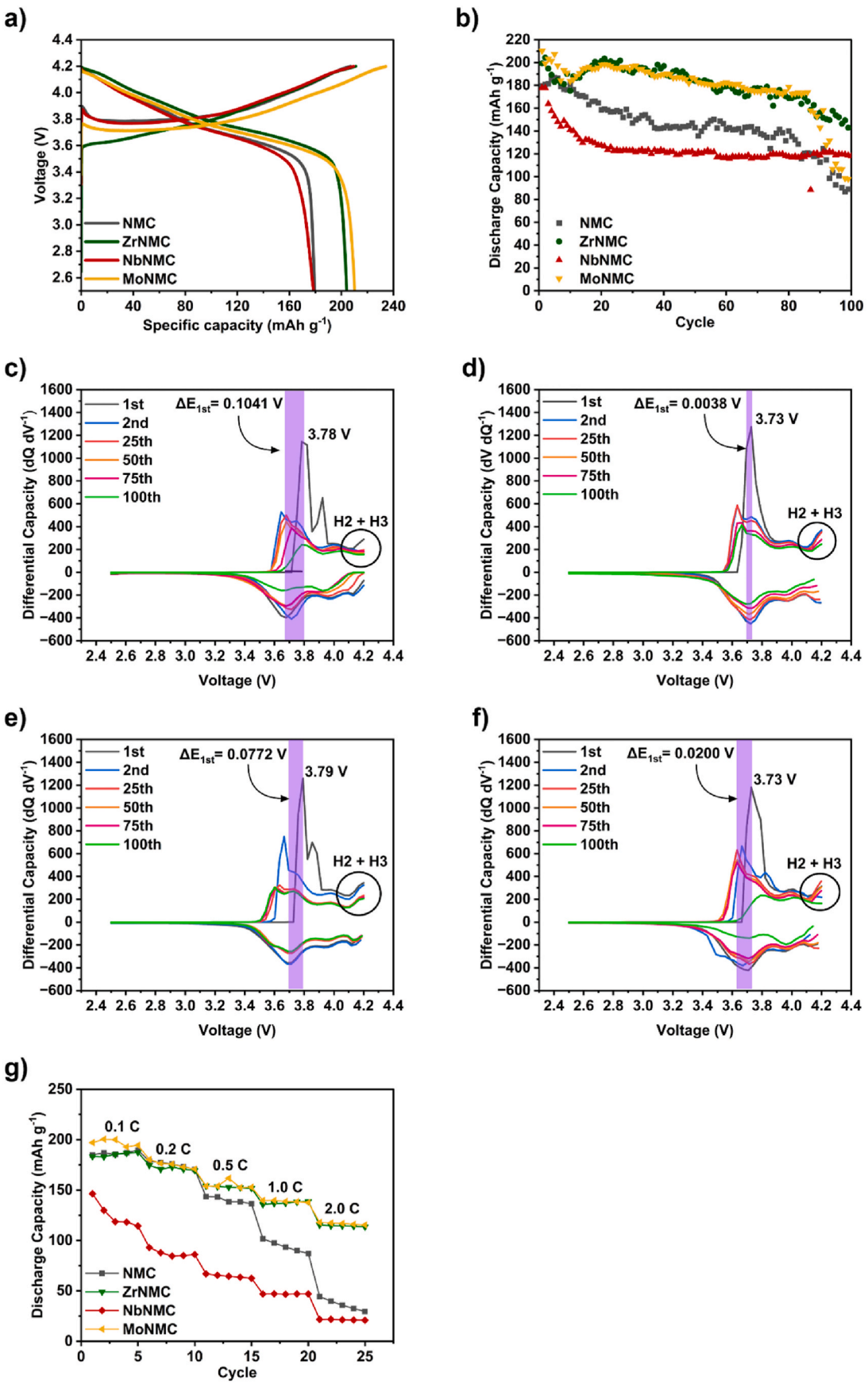

Fig. 5. (a) Initial capacity, (b) Cycling performance of NMC, ZrNMC, NbNMC and MoNMC, dQ/dV curve of (c) NMC, (d) ZrNMC, (e) NbNMC and (f) MoNMC for 1st, 2nd, 25th, 50th, 75th and 100th cycle and (g) rate capability of NMC, ZrNMC, NbNMC and MoNMC.

Table 4
Charge and discharge capacity for 1st cycle, 2nd cycle and 100th, capacity retention and initial Coulombic efficiency of NMC, ZrNMC, NbNMC and MoNMC.

Cycle	1st		100th		Capacity retention (%)	Initial Coulombic efficiency (%)
Sample	Charge (mAh g^{-1})	Discharge (mAh g^{-1})	Charge (mAh g^{-1})	Discharge (mAh g^{-1})		
NMC	207.14	179.50	90.00	89.08	49.6	89.8
ZrNMC	211.14	199.27	154.42	142.70	71.6	94.4
NbNMC	209.36	177.75	120.46	118.84	66.9	84.9
MoNMC	234.15	210.24	101.37	97.23	46.2	89.8

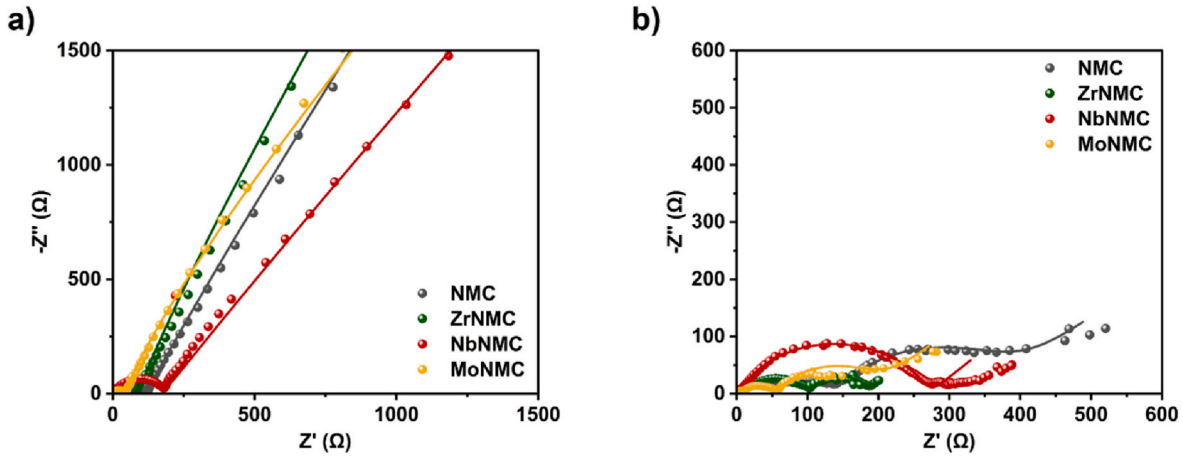

Fig. 6. Nyquist plots and equivalent circuit of all cathode materials at (a) before cycle and (b) 100th cycle.

Table 5
EIS fitting results for all cathode materials.

Sample	R_s (Ω)		R_{sf} (Ω)		R_{ct} (Ω)		R_{int} (Ω) = R_{sf} + R_{ct}	
	Before cycle	After 100th cycle	Before cycle	After 100th cycle	Before cycle	After 100th cycle	Before cycle	After 100th cycle
NMC	0.433	21.94	-	131.70	117.14	242.12	117.14	373.80
ZrNMC	0.871	0.767	-	74.62	88.14	107.46	88.14	182.08
NbNMC	0.648	1.892	-	-	-	270.03	180.28	270.03
MoNMC	0.774	3.531	-	54.88	42.49	145.22	42.49	200.10

smallest R_{int}. The significantly reduced R_{sf} and R_{ct} observed in ZrNMC indicate that Zr doping effectively stabilizes the cathode surface. The structural stabilization near the surface preserves favorable Li^+ transport pathways and enhances interfacial charge-transfer kinetics. These effects result in the lowest interfacial resistance among all samples. Meanwhile, NbNMC, only one enlarged semicircle is observed, indicating strong overlap between surface-film and charge-transfer processes; therefore, the fitted resistance represents the combined contribution of R_{sf} and R_{ct} [59]. The relatively large total interfacial resistance of NbNMC (R_{int} = 270.03 Ω) compared with ZrNMC and MoNMC is consistent with its inferior cycling stability and rate capability.

In this work, among the investigated dopants, the incorporation of Zr^{4+} into $LiNi_{0.8}Mn_{0.1}Co_{0.1}O_2$ significantly reduces cation mixing and internal polarization, which collectively contributes to improved cycling stability, high initial discharge capacity, and lower charge transfer resistance (Rct). Furthermore, the enhanced cycling performance of ZrNMC is attributed to improved structural stability, as Zr^{4+} effectively suppresses the irreversible H2/H3 phase transition that typically induces abrupt lattice contraction and expansion during high-voltage cycling. This mitigation of structural distortion reduces stress accumulation within the lattice framework. Overall, this work provides mechanistic insight into dopant-induced structural stabilization and offers a strategy for enhancing the electrochemical performance of Ni-rich layered cathode materials.

Table 6 shows a comparison between the electrochemical performance of the present high oxidation states doped Ni-rich NMC811 cathode materials and previously reported Ni-rich NMC cathode materials. While most previous reports primarily describe performance enhancement achieved through individual dopants, this study provides a comparative evaluation or multiple dopants under the same NMC811 precursor source and similar electrochemical testing conditions, enabling clearer structural and electrochemical performance to be established. The doped sample synthesized via solvent solution method in this study effectively suppresses cation disorder, enhances structural stability, and facilitates Li^+ transport, thereby demonstrates a comparable electrochemical performance, particularly ZrNMC. Further optimization is required to achieve improved cell performance, including optimization of dopant concentration, thermal treatment conditions, and electrode formulation, which may further enhance structural stability and electrochemical kinetics while maintaining the benefits observed in the present study.

4. Conclusions

A well-ordered, layer-structured doped $LiNi_{0.8}Mn_{0.1}Co_{0.1}O_2$ (NMC811) was successfully synthesized using a solvent solution method. The effect of various dopants (Zr^{4+}, Nb^{5+} and Mo^{6+}) on the structure, morphology, and electrochemical performance of NMC811 was investigated. All doped materials show a typical α-$NaFeO_2$ structure with the space group of R-3m, and successfully reduces cation mixing. Among the doped samples, ZrNMC and MoNMC exhibited high initial

Table 6
Comparison of the electrochemical performance of doped Ni-rich NMC cathode materials done by the previous studies.

Starting materials	Cathode materials	Dopant	Doping method	1st cycle (mAh g^{-1}) @ C-rate	Capacity retention (%) @ cycle number	Cut-off voltage (V)	Ref
$NiSO_4$, $CoSO_4$, $MnSO_4$, ZrO_2	$LiNi_{0.8}Mn_{0.1}Co_{0.1}O_2$	Zr	Solid-state	191.87 @ 0.2 C	74 @ 200	3.0 – 4.5	[25]
Commercial precursor $LiNi_{0.8}Mn_{0.1}Co_{0.1}O_2$, $Zr(OC_4H_9)_4$	$LiNi_{0.8}Mn_{0.1}Co_{0.1}O_2$	Zr	Sol-gel	208.4 @ 0.2 C	93.4 @ 100	3.0 – 4.3	[27]
Commercial precursor $Ni_{0.83}Co_{0.12}Mn_{0.05}(OH)_2$, nano-$ZrO_2$	$LiNi_{0.83}Mn_{0.05}Co_{0.12}O_2$	Zr	Lithiation sintering method	207.2 @ 0.1 C	94.6 @ 200	2.5 – 4.3	[35]
Commercial precursor $NMC(OH)_2$, $NMCZr(OH)_2$	$LiNi_{0.8}Mn_{0.1}Co_{0.1}O_2$	Zr	Co-precipitation	~185 @ 1 C	85 @ 100	3.0 – 4.6	[36]
$NiSO_4{\cdot}6H_2O$, $CoSO_4{\cdot}7H_2O$, $MnSO_4{\cdot}H_2O$, Nb_2O_5	$LiNi_{0.8}Mn_{0.1}Co_{0.1}O_2$	Nb	Solid-state	202.3 @ 0.1 C	90.6 @ 100	3.0 – 4.3	[28]
$Ni(NO_3)_2{\cdot}6H_2O$, $Co(NO_3)_2{\cdot}6H_2O$, $Mn(NO_3)_2{\cdot}4H_2O$, Nb_2O_5	$LiNi_{0.8}Mn_{0.1}Co_{0.1}O_2$	Nb	Solid-state	181.6 @ 1 C	94.55 @ 100	2.7 – 4.3	[29]
Commercial $LiNi_{0.8}Mn_{0.1}Co_{0.1}O_2$, $C_{12}H_{35}LiNbO_6$	$LiNi_{0.8}Mn_{0.1}Co_{0.1}O_2$	Nb	Wet chemical method	226.2 @ 0.1 C	82.6 @ 60	2.8 – 4.6	[30]
Commercial precursor $Ni_{0.8}Co_{0.1}Mn_{0.1}(OH)_2$, MoO_3	$LiNi_{0.8}Mn_{0.1}Co_{0.1}O_2$	Mo	Solid-state	213.4 @ @ 0.1 C	88.51 @ 100	2.8 – 4.3	[33]
Commercial precursor $Ni_{0.84}Co_{0.11}Mn_{0.05}(OH)_2$, MoO_3	$LiNi_{0.84}Mn_{0.05}Co_{0.11}O_2$	Mo	Solid-state	205 @ 0.1 C	89.5 @ 80	3.0 – 4.3	[34]
Commercial precursor $Ni_{0.8}Mn_{0.1}Co_{0.1}(OH)_2$, $ZrO(NO_3)_2{\cdot}xH_2O$ $C_4H_4NNbO_9{\cdot}xH_2O$ $(NH_4)_6Mo_7O_{24}{\cdot}4H_2O$	$LiNi_{0.8}Mn_{0.1}Co_{0.1}O_2$	Zr Nb Mo	Solvent solution method	199.27 @ 0.1 C 177.75 @ 0.1 C 210.24 @ 0.1 C	71.6 @ 100 66.9 @ 100 46.2 @ 100	2.5 – 4.2	**This study**

discharge capacities and better cycling performance than the undoped NMC. ZrNMC demonstrated the highest capacity retention, suppresses the irreversibility of H2/H3 phase transition, the lowest polarization, indicating that Zr^{4+} effectively enhances the performance of the NMC811 cathode material. ZrNMC exhibited low R_{ct} before cycling and after 100 cycles. Although MoNMC initially showed the lowest R_{ct} value, its R_{ct} increased significantly after prolonged cycling, which correlates with the rapid capacity fading observed during the final cycles. Overall, ZrNMC demonstrated the best electrochemical performance among all the investigated cathode materials.

CRediT authorship contribution statement

Nur Anna Lia: Writing – original draft, Visualization, Methodology, Investigation, Formal analysis, Data curation. **Kelimah Elong:** Writing – review & editing, Validation, Supervision, Project administration, Formal analysis. **Farish Irfal Saaid:** Writing – review & editing, Validation. **Lailatul Isti'adzah:** Visualization, Formal analysis. **Azira Azahidi:** Writing – review & editing. **Nurul Dhabitah Basri:** Visualization. **Nurul Atikah Mohd Mokhtar:** Writing – review & editing. **Muhamad Kamil Yaakob:** Writing – review & editing. **Muhd Firdaus Kasim:** Writing – review & editing, Validation, Supervision, Project administration, Funding acquisition, Formal analysis, Data curation, Conceptualization.

Declaration of competing interest

The authors declare the following financial interests/personal relationships which may be considered as potential competing interests: Muhd Firdaus Kasim reports financial support was provided by Malaysia Ministry of Higher Education. If there are other authors, they declare that they have no known competing financial interests or personal relationships that could have appeared to influence the work reported in this paper.

Acknowledgements

The authors would like to thank the Ministry of Higher Education Malaysia through the Fundamental Research Grant Scheme (FRGS) with code FRGS/1/2022/STG04/UITM/02/14, Faculty of Applied Sciences and Centre for Functional Materials and Nanotechnology, Institute of Science, Universiti Teknologi MARA, Shah Alam, Selangor, Malaysia for their support to this work.

Data availability

Data will be made available on request.

References

[1] L. Chen, G. Msigwa, M. Yang, A.I. Osman, S. Fawzy, D.W. Rooney, P.-S. Yap, Strategies to achieve a carbon neutral society: a review, Environ. Chem. Lett. 20 (2022) 2277–2310, https://doi.org/10.1007/s10311-022-01435-8.
[2] J. Wang, W. Azam, Natural resource scarcity, fossil fuel energy consumption, and total greenhouse gas emissions in top emitting countries, Geosci. Front. 15 (2024) 101757, https://doi.org/10.1016/j.gsf.2023.101757.
[3] F. Wang, J.D. Harindintwali, Z. Yuan, M. Wang, F. Wang, S. Li, Z. Yin, L. Huang, Y. Fu, L. Li, S.X. Chang, L. Zhang, J. Rinklebe, Z. Yuan, Q. Zhu, L. Xiang, D.C. W. Tsang, L. Xu, X. Jiang, J. Liu, N. Wei, M. Kästner, Y. Zou, Y.S. Ok, J. Shen, D. Peng, W. Zhang, D. Barceló, Y. Zhou, Z. Bai, B. Li, B. Zhang, K. Wei, H. Cao, Z. Tan, L. Zhao, X. He, J. Zheng, N. Bolan, X. Liu, C. Huang, S. Dietmann, M. Luo, N. Sun, J. Gong, Y. Gong, F. Brahushi, T. Zhang, C. Xiao, X. Li, W. Chen, N. Jiao, J. Lehmann, Y.-G. Zhu, H. Jin, A. Schäffer, J.M. Tiedje, J.M. Chen, Technologies and perspectives for achieving carbon neutrality, Innovation 2 (2021) 100180, https://doi.org/10.1016/j.xinn.2021.100180.
[4] M.Z. Najihah, F.I. Saaid, I.M. Noor, H.J. Woo, T. Winie, Iron cobalt selenide counter electrode for application in dye-sensitized solar cell: synthesis parameter, structural, electrochemical, and efficiency studies, Ionics 30 (2024) 2939–2955, https://doi.org/10.1007/s11581-024-05462-z.
[5] M. Farghali, A.I. Osman, Z. Chen, A. Abdelhaleem, I. Ihara, I.M.A. Mohamed, P.-S. Yap, D.W. Rooney, Social, environmental, and economic consequences of integrating renewable energies in the electricity sector: a review, Environ. Chem. Lett. 21 (2023) 1381–1418, https://doi.org/10.1007/s10311-023-01587-1.
[6] M.W. Rakib, A.H. Munna, T. Farooq, A. Boker, M. He, Enhancing grid stability and sustainability: energy-storage-based hybrid systems for seamless renewable integration, European Journal of Electrical Engineering and Computer Science 8 (2024) 1–8, https://doi.org/10.24018/ejece.2024.8.3.618.

[7] R. Guo, F. Wang, M. Akbar Rhamdhani, Y. Xu, W. Shen, Managing the surge: a comprehensive review of the entire disposal framework for retired lithium-ion batteries from electric vehicles, J. Energy Chem. 92 (2024) 648–680, https://doi.org/10.1016/j.jechem.2024.01.055.

[8] A. Arsyad, F.I. Saaid, M.Z. Najihah, R. Hisam, H.J. Woo, T.-Y. Tseng, T. Winie, CNT-rGO-wrapped FeCo2O4 for asymmetric supercapacitor with enhanced power density and rate capability, J. Mater. Sci. Mater. Electron. 35 (2024) 2114, https://doi.org/10.1007/s10854-024-13819-3.

[9] Y. Wang, E. Wang, X. Zhang, H. Yu, High-voltage "Single-Crystal" cathode materials for lithium-ion batteries, Energy & Fuels 35 (2021) 1918–1932, https://doi.org/10.1021/acs.energyfuels.0c03608.

[10] N. Nasajpour-Esfahani, H. Garmestani, M. Bagheritabar, D.J. Jasim, D. Toghraie, S. Dadkhah, H. Firoozeh, Comprehensive review of lithium-ion battery materials and development challenges, Renew. Sustain. Energy Rev. 203 (2024) 114783, https://doi.org/10.1016/j.rser.2024.114783.

[11] J. Zheng, W.H. Kan, A. Manthiram, Role of Mn content on the electrochemical properties of nickel-rich layered LiNi 0.8– x Co 0.1 Mn 0.1+ x O 2 (0.0 ≤ x ≤ 0.08) cathodes for lithium-ion batteries, ACS Appl. Mater. Interfaces 7 (2015) 6926–6934, https://doi.org/10.1021/acsami.5b00788.

[12] Y. Kim, W.M. Seong, A. Manthiram, Cobalt-free, high-nickel layered oxide cathodes for lithium-ion batteries: progress, challenges, and perspectives, Energy Storage Mater. 34 (2021) 250–259, https://doi.org/10.1016/j.ensm.2020.09.020.

[13] Y. Song, Y. Cui, B. Li, L. Geng, J. Yan, D. Zhu, P. Zhou, J. Zhou, Z. Yan, Q. Xue, Y. Tang, W. Xing, Revealing the origin of high-thermal-stability of single-crystal Ni-rich cathodes toward higher-safety batteries, Nano Energy 116 (2023) 108846, https://doi.org/10.1016/j.nanoen.2023.108846.

[14] L. Wang, Q. Su, W. Shi, Y. Wang, G. Wang, B. Han, J. Guo, R. Ye, G. Du, M. Zhang, W. Zhao, S. Ding, Y. Yang, B. Xu, Insights into the structural degradation and dual modification to enhance structural and cycling stability in LiNi0.8Co0.1Mn0.1O2, J. Power Sources 642 (2025) 236907, https://doi.org/10.1016/j.jpowsour.2025.236907.

[15] H. Ding, Y. Su, X. Wang, Y. Hu, X. Li, H. Zhang, G. Liu, W. Yu, X. Dong, J. Wang, X. Wang, Challenges and strategies for the cyclic stability of Ni-rich layered oxide cathode materials, J. Energy Chem. (2025), https://doi.org/10.1016/j.jechem.2025.04.039.

[16] X. Tian, Y. Zhu, Z. Tang, P. Xie, A. Natarajan, Y. Zhou, Ni-rich LiNi0.6Co0.2Mn0.2O2 nanoparticles enwrapped by a 3D graphene aerogel network as a high-performance cathode material for Li-ion batteries, Ceram. Int. 45 (2019) 22233–22240, https://doi.org/10.1016/j.ceramint.2019.07.247.

[17] Z. Ahaliabadeh, X. Kong, E. Fedorovskaya, T. Kallio, Extensive comparison of doping and coating strategies for Ni-rich positive electrode materials, J. Power Sources 540 (2022) 231633, https://doi.org/10.1016/j.jpowsour.2022.231633.

[18] M.F. Kasim, W.A.H.W. Azizan, K.A. Elong, N. Kamarudin, M.K. Yaakob, N. Badar, Enhancing the structural stability and capacity retention of Ni-rich LiNi0.7Co0.3O2 cathode materials via Ti doping for rechargeable Li-ion batteries: experimental and computational approaches, J. Alloys Compd. 888 (2021) 161559, https://doi.org/10.1016/j.jallcom.2021.161559.

[19] Y. Mu, X. Chen, H. Ming, S. Zhang, X. Zhu, J. Qiu, Oriented gradient doping of zirconium in Ni-Rich cathode to achieve ultrahigh stability and rate capability, ACS Appl. Mater. Interfaces 15 (2023) 49289–49298, https://doi.org/10.1021/acsami.3c11662.

[20] X. Li, T. Lai, A. Sheng, J. Yang, Y. Li, S. Xiao, W. Li, H. Tan, B. Huang, Effects of Nb-doping on cycle life, self-discharge and crack resistance of Ni-rich LiNi0.94Co0.02Al0.04O2 cathode for Li-ion batteries, J. Energy Storage 72 (2023) 108262, https://doi.org/10.1016/j.est.2023.108262.

[21] S.-J. Sim, S.-H. Lee, B.-S. Jin, H.-S. Kim, Improving the electrochemical performances using a V-doped Ni-rich NCM cathode, Sci. Rep. 9 (2019) 8952, https://doi.org/10.1038/s41598-019-45556-7.

[22] F. Fan, R. Zheng, T. Zeng, H. Xu, X. Wen, X. Wang, G. Tian, S. Wang, C. Zeng, W. Xiang, C. Shu, Cation-ordered Ni-rich positive electrode material with superior chemical and structural stability enabled by atomic substitution for lithium-ion batteries, Chem. Eng. J. 477 (2023) 147181, https://doi.org/10.1016/j.cej.2023.147181.

[23] H.H. Sun, U.-H. Kim, J.-H. Park, S.-W. Park, D.-H. Seo, A. Heller, C.B. Mullins, C. S. Yoon, Y.-K. Sun, Transition metal-doped Ni-rich layered cathode materials for durable Li-ion batteries, Nat. Commun. 12 (2021) 6552, https://doi.org/10.1038/s41467-021-26815-6.

[24] M. Colalongo, B. Ali, N. Vostrov, M. Ronovský, M. Mirolo, V. Vinci, C. Atzori, I. Martens, P. Kúš, A. Sartori, L. Yao, H. Jiang, T. Schulli, J. Drnec, T. Kankaanpää, T. Kallio, Operando investigation of Zr doping in NMC811 cathode for high energy density lithium ion batteries, ChemSusChem 18 (2025), https://doi.org/10.1002/cssc.202401796.

[25] K. Wu, J. Jiao, N. Li, M. Wang, G. Jia, Y.L. Lee, R. Dang, X. Deng, X. Xiao, Z. Wu, Revealing the multiple influences of Zr substitution on the structural and electrochemical behavior of high nickel LiNi 0.8 Co 0.1 Mn 0.1 O 2 cathode material, J. Phys. Chem. C 125 (2021) 10260–10273, https://doi.org/10.1021/acs.jpcc.1c01727.

[26] S.H. Akella, S. Taragin, Y. Wang, H. Aviv, A.C. Kozen, M. Zysler, L. Wang, D. Sharon, S.B. Lee, M. Noked, Improvement of the Electrochemical Performance of LiNi 0.8 Co 0.1 Mn 0.1 O 2 via Atomic Layer Deposition of Lithium-Rich Zirconium Phosphate Coatings, ACS Appl. Mater. Interfaces 13 (2021) 61733–61741, https://doi.org/10.1021/acsami.1c16373.

[27] X. Lu, Q. Mao, Y. Wang, T. Ji, Y. Zeng, Y. Xu, Y. Xia, R. Shan, P. Xu, Y. Cai, J. Yao, Effect of lithium to zirconium ratio on microstructure and electrochemical performances of LZO modified LiNi0.8Co0.1Mn0.1O2 cathode materials, Surf. Interfaces 36 (2023) 102480, https://doi.org/10.1016/j.surfin.2022.102480.

[28] Y.-R. Kim, Y.-W. Yoo, D.-Y. Hwang, T.-Y. Shim, C.-Y. Kang, H.-J. Park, H.-S. Kim, S.-H. Lee, Effect of niobium doping to enhance electrochemical performances of LiNi0.8Co0.1Mn0.1O2 cathode material, Solid State Ion 389 (2023) 116108, https://doi.org/10.1016/j.ssi.2022.116108.

[29] J. Li, M. Zhang, D. Zhang, Y. Yan, Z. Li, An effective doping strategy to improve the cyclic stability and rate capability of Ni-rich LiNi0.8Co0.1Mn0.1O2 cathode, Chem. Eng. J. 402 (2020) 126195, https://doi.org/10.1016/j.cej.2020.126195.

[30] F. Xin, H. Zhou, X. Chen, M. Zuba, N. Chernova, G. Zhou, M.S. Whittingham, Li–Nb–O Coating/Substitution Enhances the Electrochemical Performance of the LiNi 0.8 Mn 0.1 Co 0.1 O 2 (NMC 811) cathode, ACS Appl. Mater. Interfaces 11 (2019) 34889–34894, https://doi.org/10.1021/acsami.9b09696.

[31] F.A. Susai, D. Kovacheva, A. Chakraborty, T. Kravchuk, R. Ravikumar, M. Talianker, J. Grinblat, L. Burstein, Y. Kauffmann, D.T. Major, B. Markovsky, D. Aurbach, Improving performance of LiNi 0.8 Co 0.1 Mn 0.1 O 2 Cathode Materials for Lithium-Ion Batteries by doping with Molybdenum-Ions: theoretical and Experimental Studies, ACS Appl. Energy Mater. 2 (2019) 4521–4534, https://doi.org/10.1021/acsaem.9b00767.

[32] H. Konishi, M. Yoshikawa, T. Hirano, The effect of thermal stability for high-ni-content layer-structured cathode materials, LiNi0.8Mn0.1−xCo0.1MoxO2 (x = 0, 0.02, 0.04), J. Power Sources 244 (2013) 23–28, https://doi.org/10.1016/j.jpowsour.2013.05.004.

[33] J. Gou, J. Hu, Q. Xu, Q. Ran, Molybdenum ion doping for enhanced performance of high-nickel LiNi0.8Co0.1Mn0.1O2Ternary cathodess, Frontiers in Science and Engineering 5 (2025) 6–19, https://doi.org/10.54691/ewte3272.

[34] T. Sattar, S.-H. Lee, B.-S. Jin, H.-S. Kim, Influence of Mo addition on the structural and electrochemical performance of Ni-rich cathode material for lithium-ion batteries, Sci. Rep. 10 (2020) 8562, https://doi.org/10.1038/s41598-020-64546-8.

[35] Q. Li, Z. Li, S. Wu, Z. Wang, X. Liu, W. Li, N. Li, J. Wang, W. Zhuang, Utilizing diverse functions of zirconium to enhance the electrochemical performance of Ni-Rich layered cathode materials, ACS Appl. Energy Mater. 3 (2020) 11741–11751, https://doi.org/10.1021/acsaem.0c01851.

[36] M. Colalongo, B. Ali, I. Martens, M. Mirolo, E. Laakso, C. Atzori, G. Confalonieri, P. Kus, A. Kobets, X. Kong, T. Schulli, J. Drnec, T. Kankaanpää, T. Kallio, Comprehensive Study of Zr-Doped Ni-Rich cathode materials upon lithiation and Co-Precipitation synthesis steps, ACS Appl. Mater. Interfaces 16 (2024) 28683–28693, https://doi.org/10.1021/acsami.4c05058.

[37] V. Ambarwati, M.Z. Mubarok, A. Purwanto, Effect of scandium doping on the structural properties and electrochemical performance of nickel-rich cathode precursor of lithium ion-battery, Mater. Chem. Phys. 313 (2024) 128726, https://doi.org/10.1016/j.matchemphys.2023.128726.

[38] Y. He, Y. Li, Y. Liu, W. Li, W. Liu, Al-doped ZnO (AZO) modified LiNi0.8Co0.1Mn0.1O2 and their performance as cathode material for lithium ion batteries, Mater. Chem. Phys. 251 (2020) 123085, https://doi.org/10.1016/j.matchemphys.2020.123085.

[39] A.J. Haider, K.M. Chahrour, A.J. Addie, A.Q. Abdullah, P.R. Jubu, S.I. AL-Saedi, A. N. Naje, Crystallinity tuning of LCNO/graphene nanocomposite cathode for high-performance lithium-ion batteries, Mater. Sci. Eng., B 300 (2024) 117116, https://doi.org/10.1016/j.mseb.2023.117116.

[40] L. Wu, Y. Liu, D. Zhang, L. Feng, W. Qin, Improved electrochemical performance at high rates of LiNi0.6Co0.2Mn0.2O2 cathode materials by pressure-treatment, J. Solid State Chem. 289 (2020) 121487, https://doi.org/10.1016/j.jssc.2020.121487.

[41] Y. Xie, F. Guo, Y. Zhang, Multifunctional Ti-Mg co-doping strategy to enhance long term cycling performance for Ni-rich cathode materials, J. Alloys Compd. 981 (2024) 173592, https://doi.org/10.1016/j.jallcom.2024.173592.

[42] W.A.H. Wan Azizan, M.F. Kasim, K. Elong, R. Rusdi, R. Mohd Rosnan, N. Kamarulzaman, Effects of Al-dopant at Ni or Co sites in LiNi 0.6 Co 0.3 Ti 0.1 O 2 on interlayer slabs (Li–O) and intralayer slabs (TM–O) and their influence on the electrochemical performance of cathode materials, RSC Adv. 10 (2020) 40291–40299, https://doi.org/10.1039/D0RA07434A.

[43] S. Aryal, J.L. Durham, A.L. Lipson, K.Z. Pupek, O. Kahvecioglu, Roles of Mn and Co in Ni-rich layered oxide cathodes synthesized utilizing a Taylor Vortex Reactor, Electrochim. Acta 391 (2021) 138929, https://doi.org/10.1016/j.electacta.2021.138929.

[44] Y. Lu, M. Pang, S. Shi, Q. Ye, Z. Tian, T. Wang, Enhanced electrochemical properties of Zr4+-doped Li1.20[Mn0.52Ni0.20Co0.08]O2 cathode material for lithium-ion battery at elevated temperature, Sci. Rep. 8 (2018) 2981, https://doi.org/10.1038/s41598-018-21345-6.

[45] B. Jeevanantham, M.K. Shobana, S.A. Ahmed, Y.-P. Fu, W.-N. Su, B.J. Hwang, Improving high-voltage cycling and stabilizing the electrode-electrolyte interface of nickel-rich layered cathodes by magnesium doping, J. Phys. Chem. Solid. 195 (2024) 112296, https://doi.org/10.1016/j.jpcs.2024.112296.

[46] B. Jeevanantham, K.P. Abhinav, M.K. Shobana, Surface modification of TiO2 coating over single crystalline NMC-83 cathode for lithium-ion batteries, J. Phys. Chem. Solid. 205 (2025) 112825, https://doi.org/10.1016/j.jpcs.2025.112825.

[47] H.-H. Ryu, H.-W. Lim, S.G. Lee, Y.-K. Sun, Optimization of molybdenum-doped Ni-rich layered cathodes for long-term cycling, Energy Storage Mater. 59 (2023) 102771, https://doi.org/10.1016/j.ensm.2023.102771.

[48] N.V. Kosova, E.T. Devyatkina, V.V. Kaichev, Optimization of Ni2+/Ni3+ ratio in layered Li(Ni,Mn,Co)O2 cathodes for better electrochemistry, J. Power Sources 174 (2007) 965–969, https://doi.org/10.1016/j.jpowsour.2007.06.051.

[49] S. Lu, Y. Liu, Z. He, Y. Li, J. Zheng, J. Mao, K. Dai, Synthesis and properties of single-crystal Ni-rich cathode materials in Li-ion batteries, Trans. Nonferrous Met. Soc. China 31 (2021) 1074–1086, https://doi.org/10.1016/S1003-6326(21)65562-0.

[50] J. Zhang, J. Qiao, K. Sun, Z. Wang, Balancing particle properties for practical lithium-ion batteries, Particuology 61 (2022) 18–29, https://doi.org/10.1016/j.partic.2021.05.006.
[51] M.D. Bouguern, A.K. M R, K. Zaghib, The critical role of interfaces in advanced Li-ion battery technology: a comprehensive review, J. Power Sources 623 (2024) 235457, https://doi.org/10.1016/j.jpowsour.2024.235457.
[52] I.D. Yulamda, W. Widyastuti, L. Noerochim, R. Asih, M.B. Ananda, A.T. Wibisono, Y. Pradesar, R. Pornprasertsuk, U. Hashim, S. Sudaryanto, L.L. Zulfa, E.N. Falah, N. Safrida, Potential regulation strategy of molar ratio and solid-state sintering temperature on regeneration of spent lithium nickel manganese cobalt oxides (NMC 111) cathode, Mater. Chem. Phys. 338 (2025) 130658, https://doi.org/10.1016/j.matchemphys.2025.130658.
[53] F. Wu, N. Liu, L. Chen, Y. Su, G. Tan, L. Bao, Q. Zhang, Y. Lu, J. Wang, S. Chen, J. Tan, Improving the reversibility of the H2-H3 phase transitions for layered Ni-rich oxide cathode towards retarded structural transition and enhanced cycle stability, Nano Energy 59 (2019) 50–57, https://doi.org/10.1016/j.nanoen.2019.02.027.
[54] H. Zheng, Z. Wang, L. Chen, H. Jiang, C. Li, Integrating trace Ti-doping and LiYO2-coating to stabilize Ni-rich cathodes for lithium-ion batteries, Particuology 80 (2023) 74–80, https://doi.org/10.1016/j.partic.2022.12.003.
[55] A.D. Shieddieque, K. Maesaroh, G.I. Zahra, M.D. Permana, T. Takei, Irkham, A. Rifai, R. Edwin, J.A. Laksmono, S. Hidayat, I. Rahayu, Enhanced electrochemical performance of LiFePO4 by coating with metal-azolate framework-5 (MAF-5) as the cathode in lithium-ion batteries, Inorg. Chem. Commun. 176 (2025) 114322, https://doi.org/10.1016/j.inoche.2025.114322.
[56] J. Ren, Z. Liu, Y. Tang, Z. Yin, T. Yang, Z. Huang, W. Wang, W. Cui, C. Zhang, Z. Shen, Y. Liu, Y. Ren, Q. Liu, Enhancing electrochemical performance of nickel-rich NCM cathode material through Nb modification across a wide temperature range, J. Power Sources 606 (2024) 234522, https://doi.org/10.1016/j.jpowsour.2024.234522.
[57] S.J. An, J. Li, Z. Du, C. Daniel, D.L. Wood, Fast formation cycling for lithium ion batteries, J. Power Sources 342 (2017) 846–852, https://doi.org/10.1016/j.jpowsour.2017.01.011.
[58] J. Song, L. Zhu, Y. Li, E. Han, Q. Zhang, G. Chen, Z. Zhang, X. Yang, Y. He, W modification of nickel-rich ternary cathode material for efficient lithium-ion batteries, J. Electrochem. Soc. 170 (2023) 010523, https://doi.org/10.1149/1945-7111/acb0b9.
[59] M.A. Zabara, G. Katırcı, F.E. Civan, A. Yürüm, S.A. Gürsel, B. Ülgüt, Insights into charge transfer dynamics of Li batteries through temperature-dependent electrochemical impedance spectroscopy (EIS) utilizing symmetric cell configuration, Electrochim. Acta 485 (2024) 144080, https://doi.org/10.1016/j.electacta.2024.144080.